Experimental study of the shear behavior of concrete-rock interfaces under static and dynamic loading in the context of low confinement stress

Menes Badika, Sophie Capdevielle, Pascal Forquin, Dominique Saletti, Matthieu Briffaut

Engineering Structures 309 (2024) 118059

Contents lists available at ScienceDirect

Engineering Structures

journal homepage: www.elsevier.com/locate/engstruct

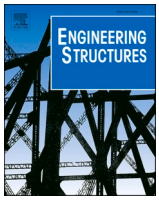

Experimental study of the shear behavior of concrete-rock interfaces under static and dynamic loading in the context of low confinement stress

Menes Badika [a], Sophie Capdevielle [a,*], Pascal Forquin [a], Dominique Saletti [a], Matthieu Briffaut [b]

[a] Univ. Grenoble Alpes, CNRS, Grenoble INP - UGA, 3SR, Grenoble, France
[b] Laboratoire de Mécanique, Multiphysique, Multiéchelle-LaMcube-UMR 9013, CNRS, Centrale Lille,University Lille, 59000 Lille, France

ARTICLE INFO

Keywords:
Concrete-rock interface
Static shear behavior
Dynamic shear behavior
Concrete-rock bonds
Roughness

ABSTRACT

Modified static and dynamic shear tests are introduced to study the shear behavior of concrete-rock interfaces under static and dynamic loading in the context of low confinement stresses. Static and dynamic shear tests of concrete-sandstone and concrete-granite interfaces are performed using these techniques. Three levels of interface roughness are considered: smooth, bush-hammered, and rough rock surfaces. The results of these tests show that in both static and dynamic regimes, the shear evolution of concrete-rock interfaces can be described according to three successive stages: the shear stress accumulation, the shear slip, and the residual shear stress stage. The main parameters driving the shear process are the concrete-rock bonds, the interface roughness, and the residual friction. However, unlike in the static shear evolution, in the dynamic shear evolution, the concrete-rock bonds and the roughness seem active in the shear stress accumulation stage. Furthermore, the correlation between the shear strength and the normal stress is stronger in static than dynamic conditions. The significance of the normal stress on the dynamic shear strength appears more important in rough concrete-granite interfaces than in the other two interfaces. Lastly, the dynamic peak shear strengths of all the interfaces tested are three to four times higher than their static counterparts.

1. Introduction

The shear failure of interfaces made of geomaterial is one of the most likely types of failure in several geotechnical structures, such as tunnels, adits, rock support systems, and concrete-gravity dams [1–3]. Thus, investigating the shear behavior of concrete-rock and rock-rock interfaces is of significant importance.

The static shear behavior of rock-rock interfaces has been extensively investigated since the seventies [4–10]. The generated literature outlines the normal stress, the roughness [6,9,11,12], the filling material between rock-rock interfaces [13], and the matching of the surfaces [14] as the most influential parameters of the shear resistance.

Compared to the literature on rock-rock interfaces, the interest in studying the shear behavior of concrete-rock interfaces is recent but growing [14–21]. Published studies highlight the influence of concrete-rock bonds on the shear resistance of interfaces when the confinement stress is low. The strong influence of the concrete-rock bonds in the shear behavior of concrete-rock interfaces is the main difference between the shear behavior of rock-rock and concrete-rock interfaces. Concrete-rock bonds influence the overall static shear behavior and the peak shear strength.

Indeed, the shear evolution of concrete-rock interfaces is usually separated into three main stages: the pre-peak, the post-peak, and the residual [17]. The pre-peak stage is mainly driven by the strength of the concrete-rock bonds across the interfaces [15,17,21]. However, this influence tends to weaken near the peak with the initiation of the degradation of the concrete-rock bonds [17]. The transition between the peak and the residual stage is characterized by the degradation of the concrete-rock bonds until their total failure [17,22]. At the same time, friction is mobilized across the interface. In the residual stage, friction is the only mechanism driving the shear evolution.

It is, however, worth noting that almost all the major experimental studies that have contributed significantly to the increasing knowledge of the shear behavior of concrete-rock interfaces are based on investigating the shear behavior of concrete-rock interfaces using a static shear loading. To move beyond this limitation, further studies are required to better understand the discrepancy between the static and dynamic shear behavior of concrete-rock interfaces. In particular, the influence of the rock type, confinement stress, and roughness level on the shear resistance needs more investigation. This research paper concentrates on the

* Corresponding author.
E-mail address: sophie.capdevielle@univ-grenoble-alpes.fr (S. Capdevielle).

https://doi.org/10.1016/j.engstruct.2024.118059
Received 2 October 2023; Received in revised form 8 March 2024; Accepted 14 April 2024
Available online 24 April 2024

experimental investigation of the dynamic shear behavior of concrete-rock interfaces under low normal stresses.

Different wave sources can generate dynamic loading [23]: seismic events, earthquakes, impacts, explosions, rockbursts, blasting, and repetitive or cyclic loading. Readers interested in cyclic loading simulating the effect of weak earthquakes are referred to [24–26]. The present research focuses on the shear loading generated upon impact, with high strain rates between 100 s^{-1} and 500 s^{-1}.

The split Hopkinson pressure bar system (SHPB) is used to generate dynamic shear loading. The SHPB can produce strain rates varying between 10^1 *to* $10^4 s^{-1}$ [23] and is an established method to study the dynamic behavior of geomaterials under compression and tension. As a reference, Dai et al. [27] and Wang et al. [28] used the SHPB system to investigate the dynamic compressive behavior of rocks and concrete. Dai et al. [29] and Huang et al. [30] used the SHPB system to study the dynamic tensile behavior of rocks. The SHPB system has also been used to investigate the dynamic shear response of materials. Huang and Xia [31], Forquin and Sallier [32], Lukić and Forquin [33], Abdul-Rahman et al. [34], and Tawfik et al. [35] used the SHPB system to conduct dynamic shear tests of rocks, concrete, and polymers. Furthermore, Dai et al. [36] and Zhang and Zhao [37] performed dynamic fracture tests of rock samples using the SHPB system.

Compared to investigating the dynamic behavior of rock or concrete under compression and tensile loading, only a few studies have investigated the dynamic shear behavior of rock-rock or concrete-rock interfaces. The remaining challenges include a better understanding of the influence of the confinement stress, the natural roughness of the interfaces, and the influence of concrete-rock bonds. Li et al. [38] proposed a dynamic shear test setup with the SHPB system to investigate the shear behavior of rock–rock interfaces. Using the proposed test setup, these authors conducted an experimental study of the dynamic shear behavior of tooth-shaped rock-rock interfaces with confinement stress. The study is limited to unbonded triangular rock-rock interfaces and does not address the more complex naturally rough rock surfaces or bonded concrete-rock interfaces. As an assessment of bonded interfaces, Zhou et al.] [39] investigated the static and dynamic tensile behavior of concrete-rock interfaces. The test performed was similar to the dynamic compression test with the SHPB system. The interfaces were tested with different orientations. Furthermore, this study provided experimental data to assess the static and dynamic tensile resistance of concrete-rock interfaces. However, the research did not consider complex interfaces like naturally rough concrete-rock interfaces. Moreover, the experimental setup did not include the application of confinement stress. Using an experimental setup similar to the SHPB compression test, Qiu et al. [40] studied the dynamic fracture of rough mortar-marble interfaces. The study showed that the roughness of the rock surface influenced the strength of the concrete-rock bonds. Without any confinement stresses, the failure occurred mainly at the interface, with the marble attached to concrete to a certain extent. The study gives interesting insights into the influence of roughness on the crack propagation speed but does not assess the influence of normal stress on the shear behavior of interfaces.

In the present research, an experimental study of the dynamic shear behavior of concrete-rock interfaces is carried out. Two types of rocks (granite and sandstone) and three levels of interface roughness (smooth, bush-hammered, and naturally rough) are considered. A specific focus on low confinement stresses, between 0.5 MPa and 2 MPa, is defined. This range of normal stresses is selected because it covers the interval of confinement stresses usually experienced by grout-based rock support systems [15] and mid-height (10 m – 60 m) concrete gravity dams. The SHPB system is used to conduct dynamic shear tests on concrete-rock samples. The challenge of such experimental testing lies in the application of a suitable confinement stress. A steel ring is used to apply the confinement stress during the test, as presented by Forquin et al. [41] for shear tests on concrete samples. This confinement ring has been adapted to applying low confinement stresses in the present research. The test setup comprises a loading phase to apply confinement stress to the interfaces and a shear phase to apply shear loading to the interfaces. Three different types of interfaces are tested: the smooth, the bush-hammered, and the natural rough concrete-rock interfaces. In addition, two different types of rocks are tested: sandstone and granite. First, the results of static shear tests are presented. These results enrich the growing literature on the static shear behavior of concrete-rock interfaces and are used in comparison with the results obtained in the study of the dynamic shear behavior of concrete-rock interfaces. Second, the results of the dynamic tests are presented. The dynamic shear evolution of the concrete-rock interfaces is described. The effect of the normal stress on the shear resistance is discussed. Finally, a comparative assessment between the static and the dynamic shear resistance of concrete-rock interfaces is discussed.

2. Materials and methods

2.1. Materials

Three different levels of roughness and two types of rocks are considered: the smooth concrete-sandstone interface, the bush-hammered concrete-granite interface, and the rough concrete-granite interface. The preparation of the rocks, the formulation of the concrete, and the subsequent combination to form the concrete-rock samples are detailed in the following sub-sections.

2.1.1. Rock

The rock samples ($30\times30\times15$ mm^3) are presented in Fig. 1. The smooth sandstone surfaces were generated using the saw-cut machine. The bush-hammered granite surfaces were created by bush-hammering smooth granite surfaces. The bush-hammering process is necessary to promote the formation of strong concrete-granite bonds [21]. The rough granite surfaces were generated by splitting granites under a three-point bending loading.

Before casting concrete, the rock surfaces were cleaned and scanned using a laser-based scanner with a point spacing of 0.025 mm and a vertical resolution of 0.05 mm. This measurement technique is one of the many adequate approaches to collecting roughness data for the investigation of the influence of roughness on the shear behavior of interfaces [42]. Moreover, this technique was particularly selected in this study because it provides a decent resolution suitable for the scope of the investigation. The fields of heights of asperities obtained were used to characterize the roughness of the rock surfaces using the 3D roughness parameter $\theta^*_{max}/(C+1)$ [43] introduced by Grasselli and Egger [8] and later modified by Tatone and Grasselli [43]. This roughness parameter was selected because it is three-dimensional, directional, and anisotropy-sensitive. Moreover, this roughness parameter is based on a strong geomechanical rationale, which considers the effect of asperities facing the shear direction and the reduction of the contact area with the shear evolution.

The maximum, minimum, and mean roughness values obtained for each surface type are presented in Table 1.

Furthermore, sandstone represents soft rocks, while granite represents hard rocks. The properties of both rocks are presented in Table 2.

2.1.2. Concrete

R30A7 concrete composition was used. This concrete composition is suitable for experimental investigations where the sample size is small. In addition, the mechanical properties of R30A7 have been investigated in several studies [32,44–47]. The mechanical properties of R30A7 and the rocks used are provided in Table 2. Table 3 shows the composition of R30A7.

2.1.3. Concrete-rock samples

The sample is a rectangular prism of $30\times30\times70$ mm^3 (Fig. 2), that contains two rock slabs at the extremities. Concrete is cast between the rock slabs, generating a sample with two bonded concrete-rock

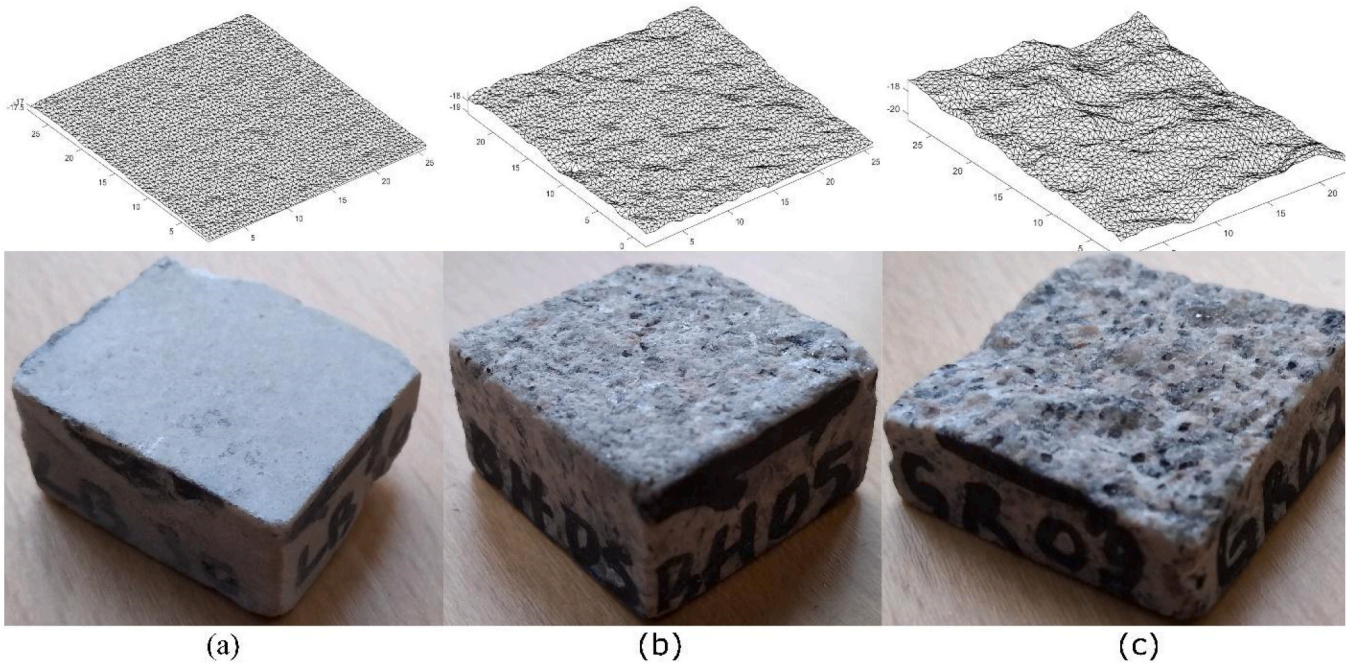

Fig. 1. Rocks slabs and plot of roughness data: (a) Sandstone (smooth), (b) granite (bush-hammered), and (c) granite (rough).

Table 1
Roughness characterization of rock surfaces.

Roughness parameter	θ^*_{max} / (C+1)		
	Max (°)	Min (°)	Mean (°)
Smooth concrete-sandstone	4.1826	2.2946	3.0889
Bush-hammered concrete-granite	8.5229	6.7343	7.6631
Rough concrete-granite	16.4642	13.0017	14.2936

Table 2
Mechanical properties of concrete and rocks.

Material	Density (kg/m3)	Compressive strength (MPa)	Young's modulus (GPa)	Poisson's ratio
Concrete	2370	30	38	0.20
Granite	2608	130	60	0.25
Sandstone	2372	71	32	0.20

Table 3
Composition of R30A7: mass of each component per unit volume of concrete.

Composition of concrete mixture	
Aggregates D 0.5/8 mm (kg/m3)	1008
Sand Dmax 1.8 mm (kg/m3)	838
Cement CEM I 52.5 N PM ES CP2 (Vicat) kg/m3	263
Water (kg/m3)	169
Density (kg/m3)	2278

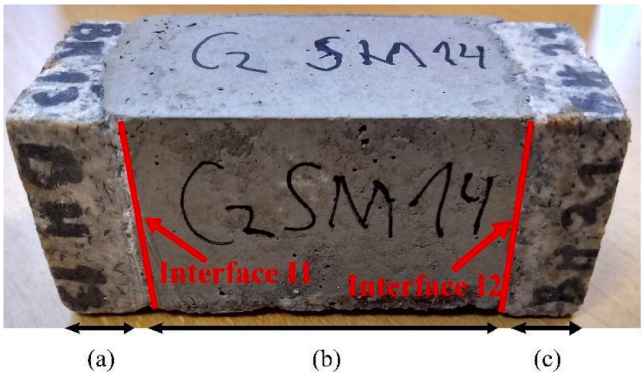

Fig. 2. Sample: (a) 15 mm rock slab, (b) 40 mm concrete, and (c) 15 mm rock slab. I1 and I2 are simplified denominations of the two interfaces of each concrete-rock sample.

Table 4
Testing program.

Interfaces	Smooth concrete-sandstone	Bush-hammered concrete-granite	Rough concrete-granite
Static tests	4	2	2
Dynamic tests	5	4	3

interfaces. The two interfaces of each sample are referred to as I1 and I2. For both the static and dynamic tests, a total of 20 samples were prepared. Table 4 illustrates the summary of the testing program.

2.2. Methods

2.2.1. Confinement loading system

This research investigates the shear resistance of concrete-rock interfaces under low confinement stress not exceeding 2 MPa in static and dynamic shear loading conditions. Therefore, it is necessary to use a confinement system adapted to generate low confinement stress, which is suitable to the setup and strain rate of both the dynamic and the static shear tests. It is worth noting that a confinement system adequate for dynamic testing with a high strain rate requires a high frequency and high accuracy measurement system.

For this purpose, the confinement ring presented by Forquin et al. [41] was selected. This confinement ring relies on strain gauges to measure the confinement stress before, during, and after the shear test. This measurement system is very convenient for static and dynamic tests. Through numerical simulations in Abaqus, the geometry of the confinement ring presented by Forquin et al. [41] was modified to make

it suitable for applying low confinement stresses. Furthermore, the elastic limit of the ring in the x and z directions was also determined. As a result, two confinement rings with thicknesses of 5 mm and 7.5 mm were manufactured to generate confinement stresses below 0.5 MPa and 2 MPa, respectively. The other measurements of the ring are presented in Fig. 3.

2.2.2. Operation of the confinement ring

The operation of the confinement ring to apply the confinement stress to the sample proceeds in three phases. In the first phase, a force F_Z is applied to the confinement ring, generating an elastic deformation. The sample is inserted into the elastically deformed ring in the second phase. In the last phase, the applied force F_Z is released, and the ring, unable to recover its initial state, confines the sample with the force F_X (Fig. 4). These phases mean that the confinement ring is a passive confinement system that cannot apply an extra loading during the shear tests but can react to the dilation of the sample. The computation of the confinement load during the operation of the ring can be summarised in Eq. (1). For the complete mathematical formulations of the operation of the ring, the interested reader is referred to Forquin et al. [41].

The coefficients α_i and β_i are determined by the ring calibration. This calibration involves deforming the ring elastically by applying loads in the x and z direction using an electromechanical press and measuring the elastic deformation recorded in the strain gauges. From the calibration, relationships between the deformation of the ring recorded in the strain gauges with the applied forces F_X ($F_X = \alpha_i^{-1}\varepsilon_i$) and F_Z ($F_Z = \beta_i^{-1}\varepsilon_i$) are established. Consequently, the confinement of the sample can be monitored before, during, and after the tests, be they static or dynamic (Fig. 5). Calibration curves are presented in Fig. 6. Table 5 shows the coefficients α and β.

$$\varepsilon_i = \alpha_i F_X + \beta_i F_Z \tag{1}$$

Notably, g1-g4 in Fig. 4 and Fig. 5 represent the strain gauges. The strain gauges are specifically selected because they are suitable for collecting data with high accuracy and high frequency.

2.2.3. Static test

2.2.3.1. Test setup. The static shear test setup follows the basic concepts of the conventional direct shear test: it consists of applying the confinement stress using the modified confinement ring, followed by applying the shear loading using the electromechanical press. Throughout the test, the normal stress is monitored using the deformation of the ring collected by the strain gauges.

The test is carried out with a velocity of 0.2 mm/min, as suggested by the International Society of Rock Mechanics [48]. The test is stopped after a shear displacement of 3 mm.

This displacement guarantees the failure of both interfaces and a subsequent post-peak phase.

The static tests were carried out in the 3SR laboratory at the University Grenoble Alpes, and the electromechanical press used was Instron 100 kN.

Fig. 7 illustrates the static shear test setup.

2.2.3.2. Computation of the static shear evolution. After the test, the average shear resistance of the interfaces is computed using the force applied by the electromechanical press and the sum of the two surfaces of the interfaces, see Eq.(2).

$$\tau_{shear}(t) = F_{axial}(t)/S_{\text{int}} \tag{2}$$

where $\tau_{shear}(t)$ is the mean shear stress at both interfaces, $F_{axial}(t)$ is the applied force, S_{int} is the area of the interfaces.

The confinement stress is deduced by processing the data recorded in the strain gauges and using the relationships between the applied forces and the deformation of the ring determined during the calibration of the ring. The results of the static shear tests are presented in the Section 3.

2.2.4. Dynamic shear test setup

2.2.4.1. Test setup. The concept of the dynamic shear test is similar to the idea of the static shear test. The only difference is the application of the shear loading using the split Hopkinson pressure bar system (Fig. 8). The SHPB system used is composed of an input bar with two output bars. The bars are made of high-strength aluminum alloy. The input bar has a diameter of 45 mm and a length of 1200 mm, while the output bars have a diameter of 20 mm and a length of 1200 mm. The projectile is also made of the same aluminum alloy and has a diameter of 45 mm and a length of 370 mm. The projectile is launched through a steel barrel using a gas gun. The stress wave in the input bar is measured at two locations using strain gauges mounted in a full bridge (g5 and g6 in Fig. 8). The transmitted stress wave in each of the output bars is measured in one location using strain gauges in full bridge mode (g7 and g8 in Fig. 8). The input bar is put in contact with the concrete part of the sample. In contrast, the output bars connect with the rock part of the sample.

Furthermore, a disc-like pulse shaper made of lead of inner and outer diameters equal to 38 mm and 45 mm with a thickness of 1 mm is attached to the impacted end of the input bar. This pulse-shaping technique is essential to the mechanical balance of the sample. This mechanical balance is important to avoid a sudden discharge of impact energy in the concrete part of the sample, which might generate cracks in the concrete before shearing the interfaces.

Moreover, it is worth noting that the length and, therefore, the mass of the striker bar was tailored based on a similar experimental work [34] such that the stress wave generated by an impact at approximately 8 m/s has enough energy to shear the two concrete-rock interfaces of the sample. This means that all the dynamic shear test results presented in this study represent a complete failure of the two interfaces of each sample tested due to the first incident wave.

2.2.4.2. Computation of the dynamic shear stress. In the testing method using the SHPB system involving an input and an output bar, it is important to verify if the mechanical equilibrium of the sample is achieved. This equilibrium guarantees the one-dimensionality of the stress wave without dispersion and makes using the unidimensional stress wave theory possible. Furthermore, the unidimensional stress wave theory permits the use of simple formulas for the computations associated with the tests. However, achieving stress equilibrium is challenging for low-impedance and brittle materials Gary and Mohr [49].

Concrete and rock separately are brittle and low-impedance materials, but in this experimental study, neither concrete nor rock is tested directly; instead, the interfaces between them are tested. Compared to concrete and rocks, the concrete-rock interfaces have even lower impedance. These latter and the local and progressive nature of the

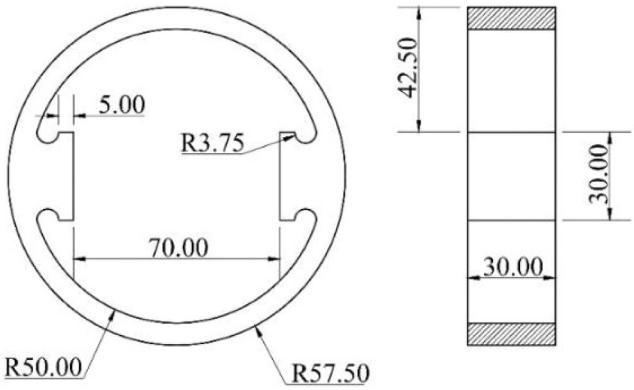

Fig. 3. Confinement ring.

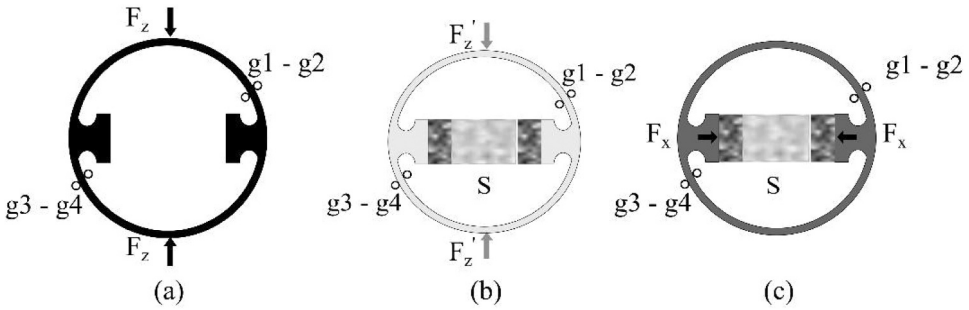

Fig. 4. Confinement of the sample:. (a): compression of the ring, (b) insertion of the sample (S), and (c) application of normal stress to the sample.

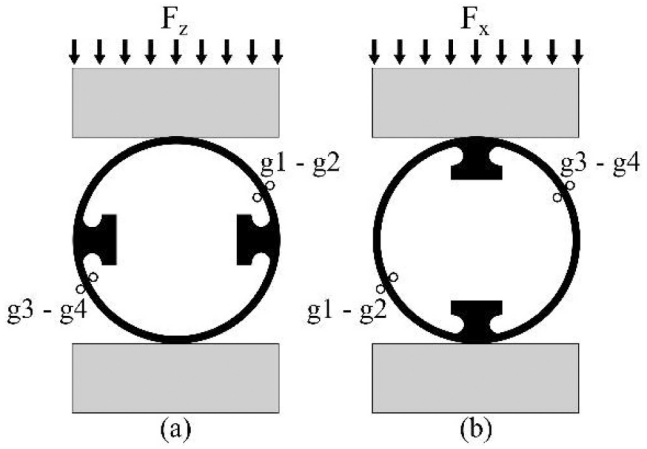

Fig. 5. Calibration of the ring: and (a) $\alpha_i = \boldsymbol{0}$ in Eq. (1) which means $\boldsymbol{F_Z = \beta_i^{-1}\varepsilon_i}$ and (b) $\beta_i = \boldsymbol{0}$ in Eq. (1) consequently $\boldsymbol{F_X = \alpha_i^{-1}\varepsilon_i}$.

shear process make achieving the stress equilibrium states highly unrealistic. Li et al. [38] and Tawfik et al. [35] also present similar conclusions.

With these two considerations, only the stress wave signals recorded in the output bars are used to compute the shear behavior of the interfaces according to Eq.(3).

$$\tau_{\text{int}}(t) = F_{tr}(t)/S_{\text{int}} = S_{bar} \quad E_{bar}\varepsilon_{tr}(t)/S_{\text{int}} \tag{3}$$

where τ_{int} is the shear stress at each interface, $F_{tr}(t)$ is the force computed from the transmitted bar, S_{int} is the area of the interface, S_{bar} is the cross-section area of the bar, E_{bar} is the elastic modulus of the bar, and $\varepsilon_{tr}(t)$ is the strain history recorded in the gauges associated with the transmitted bar (g7 and g8 in Fig. 8).

3. Test results

The summary of the results of the static and dynamic tests is presented in Table 6. Where τ represents the peak shear strength and σ the normal stress at a peak during the shear history. Two shear evolutions corresponding to two interfaces are assessed for each sample tested. This is possible because each sample comprises two interfaces (refer to Section 2.1.3 and Fig. 2).

Furthermore, the linear fitting adopted for this analysis attempts to fit the Mohr-Coulomb failure criterion. This failure criterion is among the most used and recommended in the literature. Since this study focuses on investigating the dynamic shear behavior of concrete-rock interfaces, more dynamic shear tests are performed. The static shear tests are designed to validate the recent findings of the static shear behavior of concrete-rock interfaces and to provide data for a fair comparative

Table 5
Gauges coefficient after calibration.

Stain gauges	Coefficient	Ring 0.5 mm thick	Ring 7.5 mm thick
Gauges g1	$\alpha 1$	- 0.97E-06	-0.43E-06
	$\beta 1$	1.05E-06	0.48E-06
Gauges g2	$\alpha 2$	1.15E-06	0.55E-06
	$\beta 2$	-1.05E-06	-0.50E-06
Gauges g3	$\alpha 3$	-1.00E-06	-0.43E-06
	$\beta 3$	1.10E-06	0.48E-06
Gauges g4	$\alpha 4$	1.11E-06	0.52E-06
	$\beta 4$	-1.01E-06	-0.44E-06

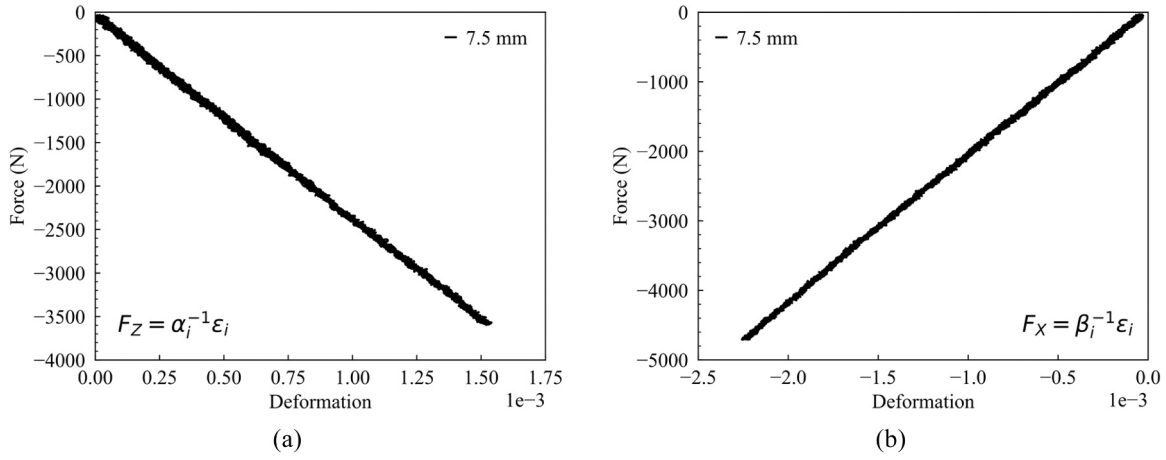

Fig. 6. Calibration curves for the correlation between the deformation of the ring and (a) the force applied by the ring to the sample or (b) the force applied to deform the ring.

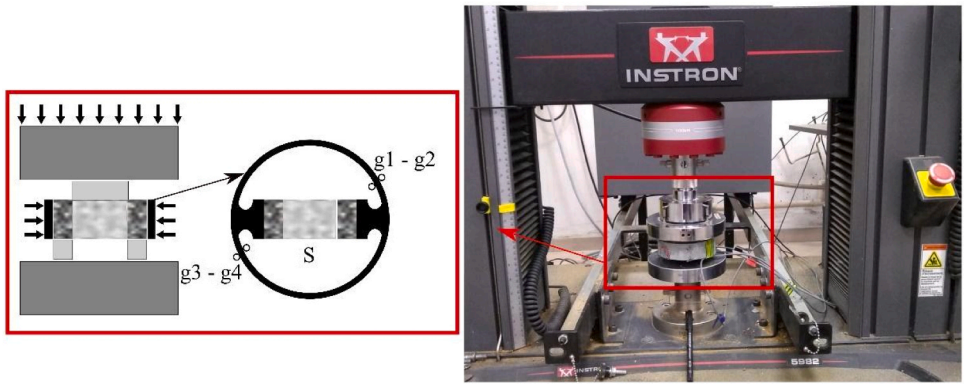

Fig. 7. Static shear test setup.

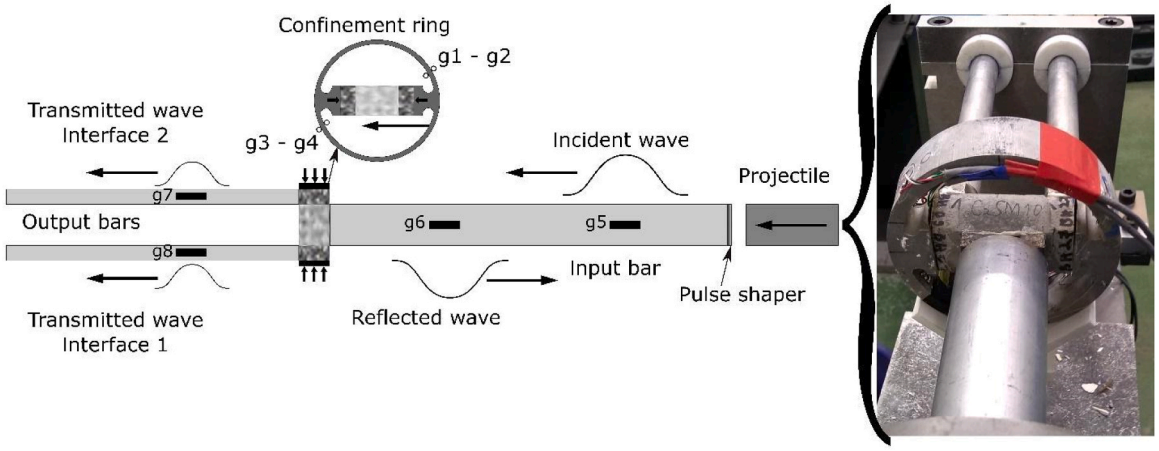

Fig. 8. Dynamic shear test setup.

Table 6
Results of static and dynamic tests.

Tests	Interfaces	Sample ID	σ_1 [MPa]	τ_1 [MPa]	σ_2 [MPa]	τ_2 [MPa]
Static	Smooth concrete-sandstone	StatSCS1	0.37	1.99	0.89	2.17
		StatSCS2	1.68	4.07	4.58	5.03
		StatSCS3	0.47	2.30	1.81	3.23
		StatSCS4	1.44	2.32	2.91	6.18
	Bush-hammered concrete-granite	StatBHCG1	0.37	1.98	0.93	2.50
		StatBHCG2	1.42	3.12	2.59	2.97
	Rough concrete-granite	StatRCG1	0.63	2.09	1.03	2.18
		StatRCG2	1.21	1.89	1.60	3.74
Dynamic	Smooth concrete-sandstone	DynSCS1	1.63	11.77	1.69	11.42
		DynSCS2	1.16	13.45	1.37	14.11
		DynSCS3	0.41	11.95	0.44	10.79
		DynSCS4	0.34	7.67	0.31	11.25
		DynSCS5	1.04	8.42	0.97	8.60
	Bush-hammered concrete-granite	DynBHCG1	1.39	9.28	1.35	10.64
		DynBHCG2	1.31	11.36	1.29	13.86
		DynBHCG3	0.51	9.75	0.56	12.47
		DynBHCG4	0.48	9.17	0.49	9.99
	Rough concrete-granite	DynRCG1	1.57	11.99	1.44	11.99
		DynRCG2	1.38	13.90	1.39	10.96
		DynRCG3	0.52	6.45	0.57	7.98

assessment between the static and the dynamic shar resistance of concrete-rock interfaces. Such a fair comparative assessment must be free of scale effect and rely upon the same confinement system.

3.1. Quasi-static tests

3.1.1. Smooth concrete-sandstone interfaces

Four samples are tested for the smooth concrete-sandstone tests, corresponding to eight interfaces. The results of two interfaces, one from sample StatSCS2 and the other from sample StatSCS4, are not considered in the subsequent analysis because the peak shear strength occurs at a

confinement stress superior to 2 MPa, which is set as the limit for this experimental study.

Fig. 9(a) shows a typical shear evolution of smooth concrete-sandstone interfaces. This behavior is discussed in Section 4.1.1.

The outcomes of the tests show that the shear stress increases with the normal stress (Fig. 9(b)), with a correlation coefficient of 0.60. The cohesion and friction angle are 1.57 MPa and 44.89°. For the normal stress varying from 0.37 MPa to 1.81 MPa, the shear strength obtained is between 1.99 MPa and 4.07 MPa.

3.1.2. Bush-hammered concrete-granite interfaces

Only three of the four interfaces tested are used to analyze the shear evolution. The result of the fourth interface (StatBHCG2) is not considered because the peak shear strength occurred at a confinement stress of 2.59 MPa, which is above the limit of 2 MPa.

Fig. 10 (a) shows a typical shear evolution of the bush-hammered concrete-granite interface. Section 4.1.1 presents a further discussion.

The graph of the peak shear strength in terms of the normal stress reports a correlation coefficient of 0.99 (Fig. 10 (b)). The cohesion and the friction angle are 1.56 MPa and 46.9°. Therefore, the shear strength varies between 1.98 MPa and 3.12 MPa when the normal stress is between 0.37 MPa and 1.42 MPa.

3.1.3. Rough concrete-granite interfaces

The shear evolutions of the two samples tested (StatRCG1 and StatRCG2) are presented in Fig. 11. Section 4.1.1 presents more discussion.

The shear tests of rough concrete-granite interfaces were stopped before the 3 mm of shear displacement, which was set as the limit for the static shear test to ensure that the confinement stress does not increase beyond the elastic limit of the ring.

Fig. 12 shows the peak shear strength in terms of normal stress. The correlation coefficient is 0.56. The cohesion and the friction angle are 0.71 MPa and 57.6°. Therefore, the Shear strength varies between 1.89 MPa and 3.74 MPa for the normal stress changing between 0.63 MPa and 1.60 MPa.

3.2. Dynamic tests

3.2.1. Smooth concrete-sandstone interfaces

Two typical shear evolutions are presented in Fig. 13. Where I1 and I2 represent the two interfaces composing each sample. Section 4.1.2 discusses the results of these tests.

Fig. 14 shows the evolution of the peak shear strength in terms of normal stress. The coefficient of correlation is 0.14. The peak shear strength varies between 7.67 MPa and 14.11 MPa when the normal stress is between 0.31 MPa and 1.69 MPa.

3.2.2. Bush-hammered concrete-granite interfaces

A typical shear evolution is presented in Fig. 15 (a).

The evolution of the peak shear strength in terms of the confinement stress is presented in Fig. 15 (b). The correlation coefficient is 0.07. The peak shear strength varies between 9.17 MPa and 13.86 MPa for the normal stress between 0.48 MPa and 1.39 MPa.

3.2.3. Rough concrete-granite interfaces

Fig. 16 (a) shows a shear evolution of rough concrete-granite interfaces.

Fig. 16 (b) illustrates the evolution of the peak shear strength in terms of confinement stress. The correlation coefficient is 0.81. The cohesion and the friction angle are 4.42 MPa and 79.42°. Therefore, the peak shear strength obtained varies between 6.45 MPa and 13.90 MPa when the normal stress is between 0.52 and 1.57 MPa.

4. Discussion

4.1. Description of the shear evolution

Contrary to the conventional direct shear test [21,48], in the static and dynamic shear tests performed in the present experimental study, two interfaces are tested with a single source of shear loading.

The consequence of this test configuration means that the shear evolutions of the two interfaces (I1 and I2) of each tested sample are intertwined, making it difficult to separate them completely. This difficulty is principally due to the local and progressive nature of the shear behavior of concrete-rock interfaces submitted to low normal loading. In the discussion presented in the following section, a reasonable assumption is adopted considering the successive failure of the concrete-rock bonds of the weaker interface, followed by the failure of the concrete-rock bonds of the stronger interface.

4.1.1. Static shear evolution of concrete-rock interfaces

The shear evolution of interfaces under static loading usually consists of three principal stages: the shear stress accumulation, the shear slip, and the residual shear stress. Similar separations of the shear evolution of concrete-rock interfaces are also presented in Saiang et al. [15],

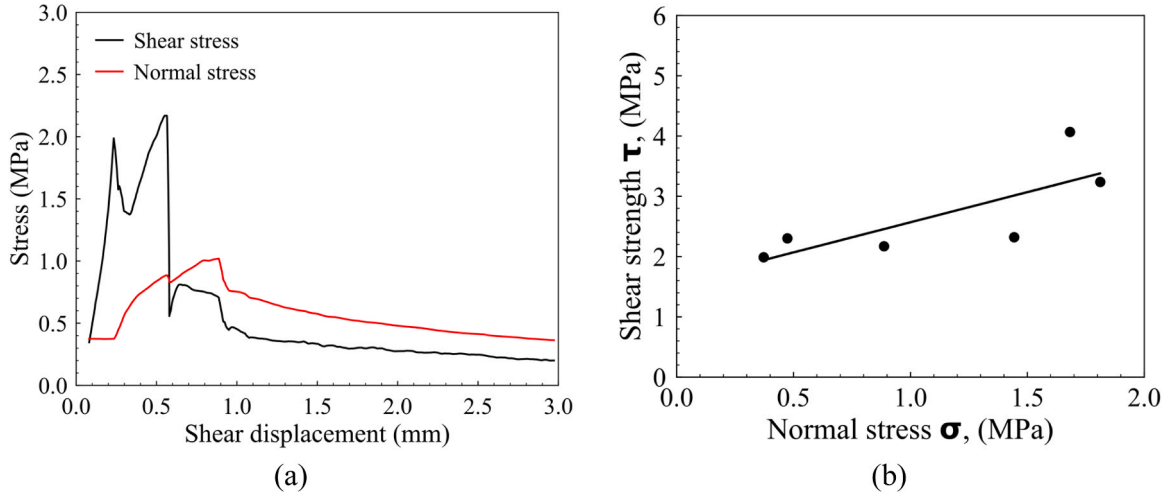

Fig. 9. (a) Typical static shear evolution of smooth concrete-sandstone interfaces (sample StatSCS1) and (b) Best fit for static peak shear strength – normal stress of smooth concrete-sandstone interfaces ($c = 1.57$**MPa** and $\phi_i = 44.89°$ **with an** $R^2 = 0.60$): two results are discarded because they occur at confinement stress above 2 MPa.

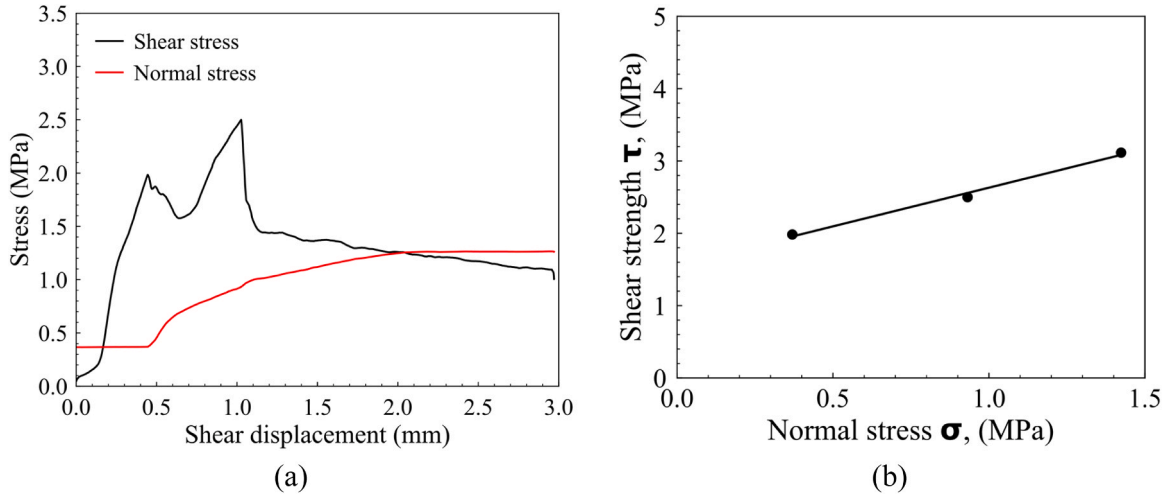

Fig. 10. (a) Typical static shear evolution of bush-hammered concrete-granite interfaces (sample StatBHCG1) and (b) Best fit for static peak shear strength – normal stress of bush-hammered concrete-granite interfaces ($c = 1.56$MPa and $\phi_i = 46.9°$ with an $R^2 = 0.99$): one result is discarded because it occurs at confinement stress above 2 MPa.

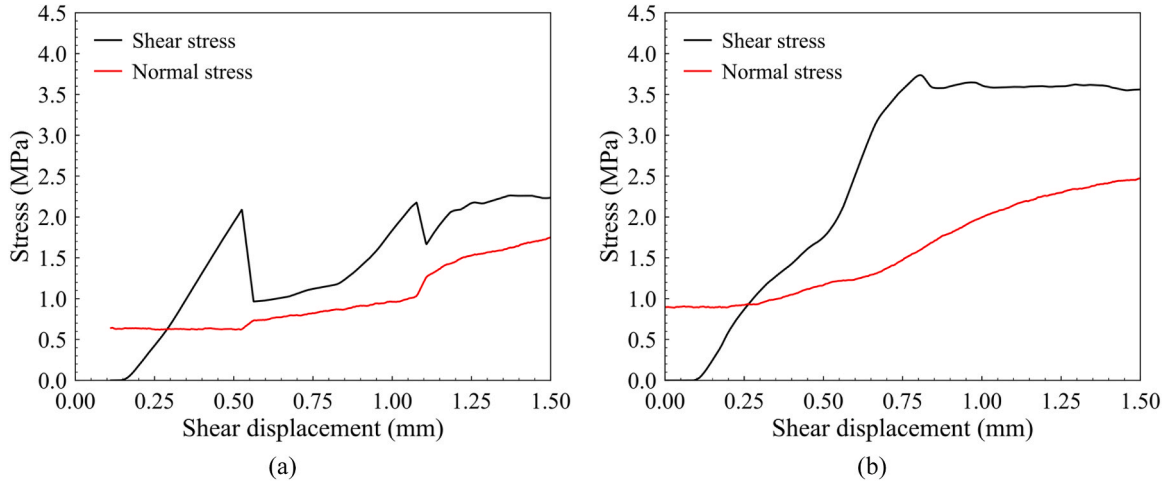

Fig. 11. Static shear evolution of rough concrete-granite interfaces: (a) StatRCG1 and (b) StatRCG2.

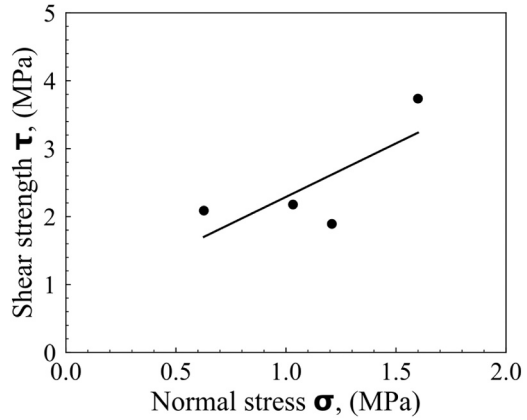

Fig. 12. Best fit for static peak shear strength – normal stress of rough concrete-granite interfaces. ($c = 0.71$ MPa and $\phi_i = 57.6°$ with an $R^2 = 0.56$).

Moradian et al. [16], Tian et al. [17], Krounis et al. [14], Mouzannar et al. [18], and Badika et al. [21].

In the first part (Fig. 17, OAB), the shear stress increases with applying the shear loading up to a peak shear strength and then drops immediately to a local residual shear strength. These two phases constitute the shear stress accumulation phase (Fig. 17, OA) and the shear slip phase (Fig. 17, AB). The peak of this part shows that the concrete-rock bonds at one interface begin to fail progressively and are substituted by friction as the driving shear mechanism. This first part indicates the failure of one interface of the sample. Meanwhile, the confinement stress remains constant. No significant normal displacement accompanies the shear evolution in this part. It is worth noting that the normal displacement or dilation of the sample would be evidenced by an increase in the confinement stress since the confinement ring is a passive confinement system that can only increase the confinement stress as a reaction to the dilation of the sample. Such a sample dilation can easily be back-calculated using the correlation relationships determined during the calibration of the ring. Implicitly, the increase in the confinement stress is equivalent to the increase in the loading F_X (refer to Section 2.2.1 and Section 2.2.2 and Fig. 5), using Eq.(1), with $F_Z = 0$, one can determine the deformation of the ring ε_i, from this deformation the dilation of the sample can be calculated.

In the second part (Fig. 17, BCD), the second interface, which did not fail in the first part of the test, goes through the same shear process as the interface that failed in the first part. The shear stress increases with the

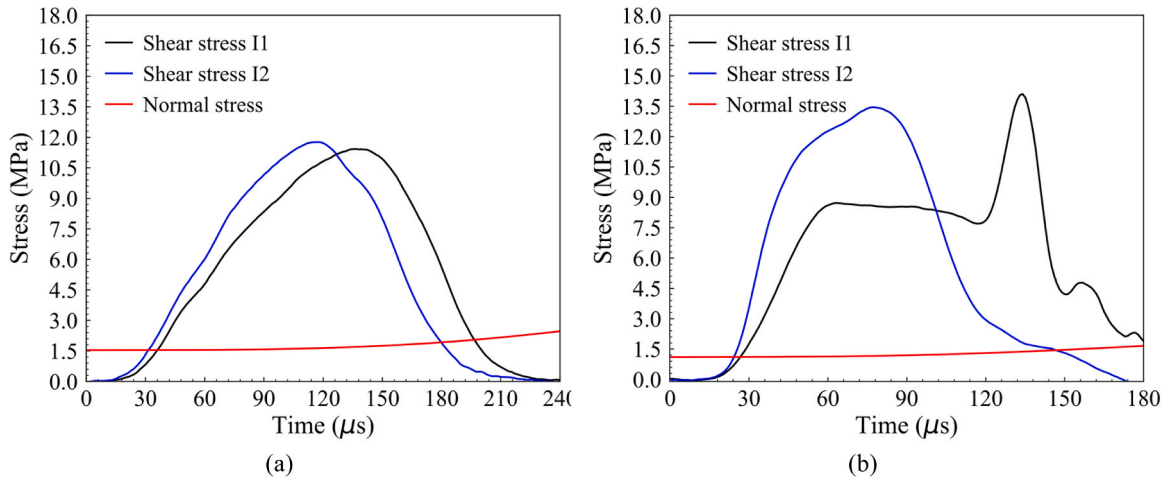

Fig. 13. Dynamic shear evolution of smooth concrete-sandstone interfaces: (a) DynSCS1 and (b) DynSCS2.

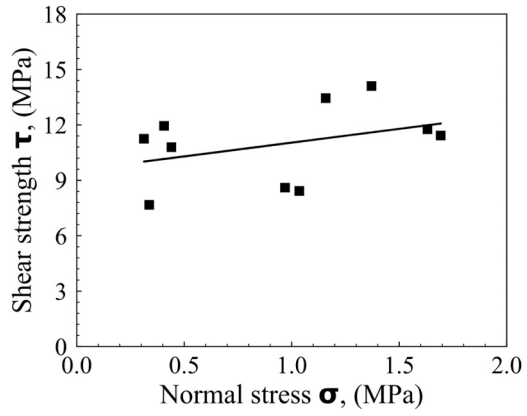

Fig. 14. Best fit for dynamic peak shear strength – normal stress of smooth concrete-sandstone interfaces (**with an $R^2 = 0.14$**).

application of the shear loading, with the concrete-rock bonds controlling the shear evolution. This process continues until the shear loading exceeds the resistance of the concrete-rock bonds and causes them to fail progressively. This failure culminates in the second peak of the shear evolution. Afterward, friction gradually substitutes the concrete-rock bonds as the primary mechanism of the shear evolution. This step completes the second cycle of stress accumulation and the shear slip stage. It is worth noticing that the confinement stress increases in the second part of the shear evolution. This increase is expected because, during the test, the central part of the sample is the only one submitted to the shear loading. To proceed, the shear displacement of the central part of the sample requires a normal displacement in the lateral part. This increase in the normal displacement leads to a dilation of the sample, against which the ring resists, causing an increment in the confinement stress.

In the third part (Fig. 17, DE), both interfaces have reached a stage where friction controls the shear evolution. As a result, the shear stress decreases to reach the residual shear strength. At this part, the confinement stress decreases or reaches a plateau.

Due to the extra complexity the roughness adds, the static shear behavior of rough concrete-rock interfaces can present some peculiarities.

For the case of low confinement stress, the shear failure evolves mainly at the interface with a shear motion characterized as "*riding along the asperities*," which means that the rock and concrete slabs slide along each other with no significant damage in neither concrete nor rock. This motion can generate significant normal displacement in the case of rough granite interfaces. This increase of normal displacement leads to a dilation of the sample, against which the ring resists increasing the

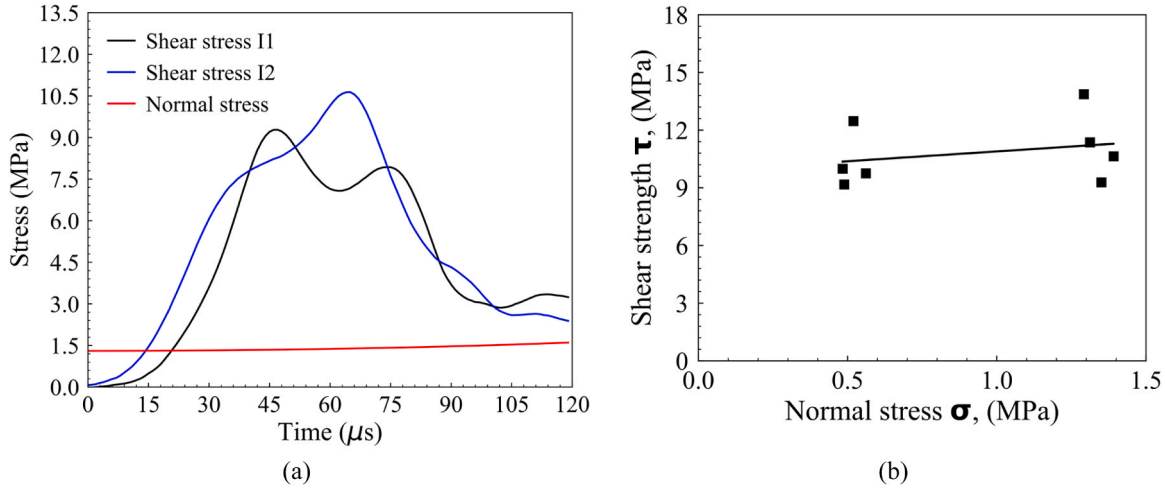

Fig. 15. (a) Dynamic shear evolution of bush-hammered concrete-granite interfaces (DynBHCG1) and (b) Best fit for dynamic peak shear strength – normal stress of bush-hammered concrete-granite interfaces (**with an $R^2 = 0.07$**).

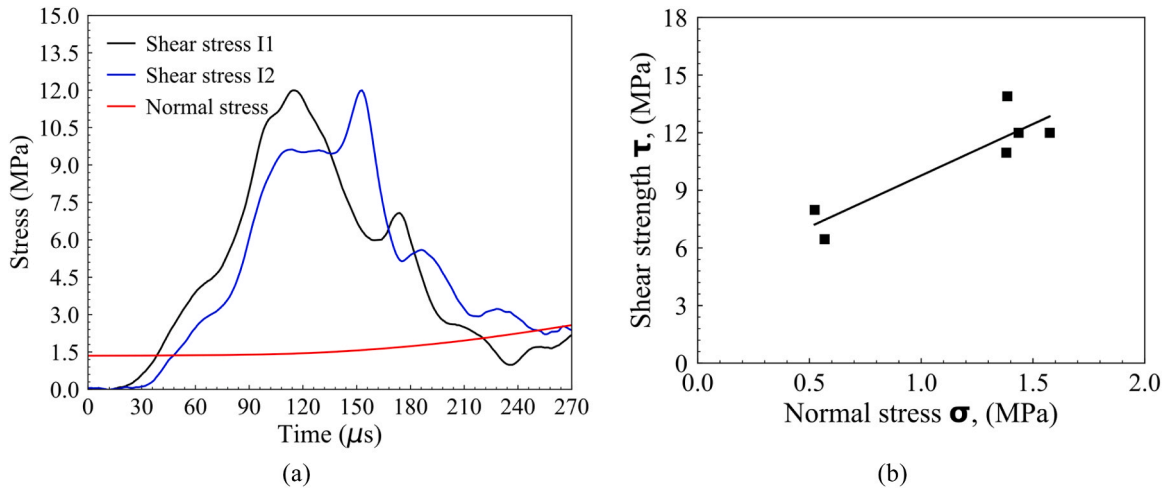

Fig. 16. (a) Dynamic shear evolution of rough concrete-granite interfaces (DynRCG1) and (b) Best fit for dynamic peak shear strength – normal stress of rough concrete-granite interfaces ($c = 4.42$ **MPa** and $\phi_i = 79.42°$ **with an** $R^2 = 0.81$).

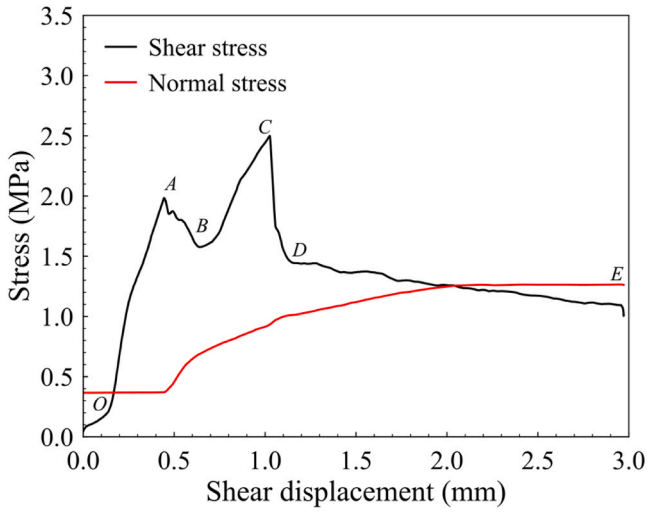

Fig. 17. Static shear evolution of concrete-rock interface (sample StatBHCG1).

confinement stress. The increase in the confinement stress leads to an increase in the shear resistance of the interfaces; this justifies the high residual stress recorded in the shear evolution of the rough concrete-granite interfaces compared to the peak shear strength (Fig. 18). The increase in the confinement and the consequent increase in the residual shear stress constitute the first possible peculiarity when analyzing the result of the static shear test of rough granite interfaces using the confinement ring. The second peculiarity observed is the lack of shear slip after the first peak shear strength. The complexities related to the roughness of the interfaces drive the competition of the shear resistance between the two interfaces. In this case, the shear slip stage of the first interface stops right after initiating because of the beginning of the stress accumulation stage in the second interface, see Fig. 18 (b).

Fig. 18 (a) and Fig. 18 (b) show the two peculiarities of the shear evolution of rough concrete-granite interfaces.

4.1.2. *Dynamic shear evolution of concrete-rock interfaces*

The dynamic shear evolution of concrete-rock interfaces maintains the three-stage division presented in the description of the static shear evolution of concrete-rock interfaces. It is worth pointing out that the dynamic shear evolution is presented in terms of time and not displacement. Nevertheless, the stages can be separated by observing the characteristic markers of the shear evolution, principally the peak and residual shear strength.

The first part of the dynamic shear evolution happens before the peak shear strength (Fig. 19 (a), OA). The curve of the shear evolution in this pre-peak part has a more curvilinear shape. This curve differs from the more linear form recorded in the pre-peak part of the static shear

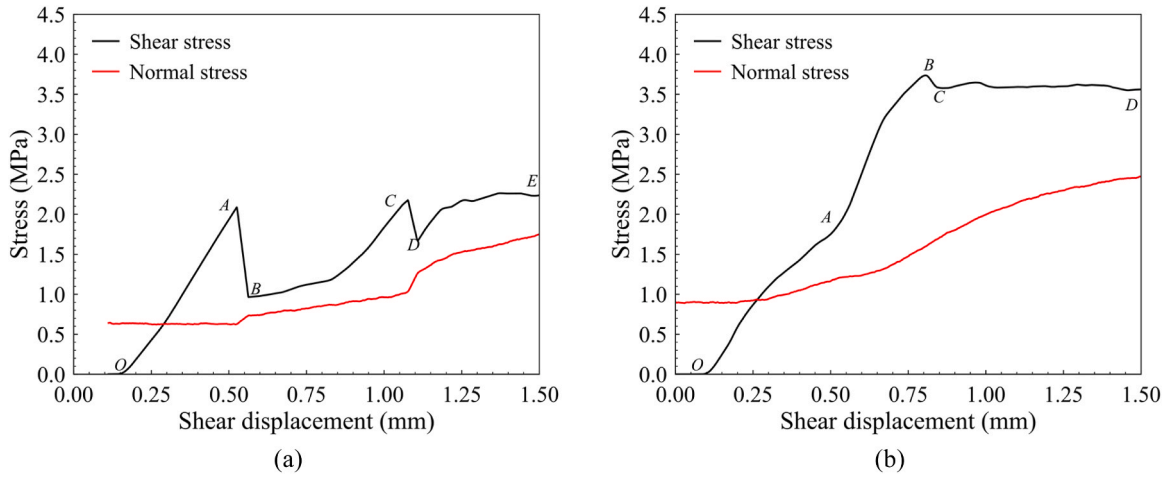

Fig. 18. Static shear evolutions of rough concrete-granite interface: (a) StatRCG1 and (b) StatRCG2.

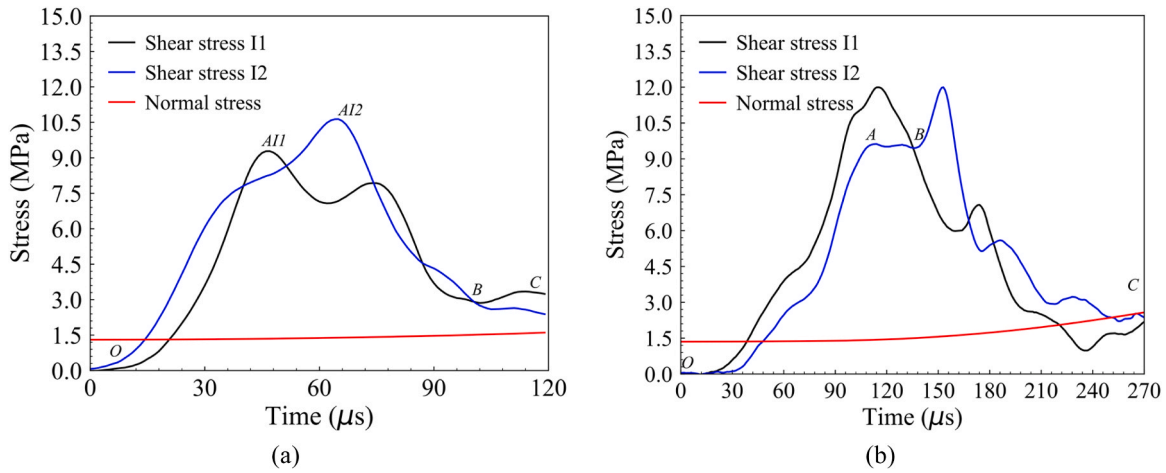

Fig. 19. (a) Dynamic shear evolution of concrete-rock interface (sample DynBHCG1) and (b) Dynamic shear evolution of concrete-rock interface (sample DynRCG1).

evolution (Fig. 17 and Fig. 18). This difference could indicate a double mobilization of concrete-rock bonds and friction compared to the mobilization of concrete-rock bonds in the static shear evolution. This part corresponds to the shear stress accumulation stage.

The second part of the dynamic shear evolution develops between the peak shear strength and the beginning of the residual shear stress stage (Fig. 19 (a), AB). This part is equivalent to the shear slip stage. The shear loading starts to overcome the resistance against the shear motion generated by the concrete-rock bonds and the roughness of the interface. The failure of the concrete-rock bonds and the reduction of the influence of roughness in this part are progressive.

The residual shear stress stage depends on the residual friction of the interface (Fig. 19 (a), BC).

Peculiarities related to the dynamic shear evolution of concrete-rock interfaces are presented hereafter.

First, compared to the static shear evolution of concrete-rock interfaces, the confinement stress also increases in the dynamic shear evolution of concrete-rock interfaces because of the dilation of the lateral part of the sample to allow the shear motion of the concrete part of the sample.

Second, the shear evolution at both interfaces does not reach the peak shear strength simultaneously. The local aspect of the shear resistance of the interfaces can explain this difference. The local shear resistance of the interface depends mainly on two factors: the local roughness of the interface and the local strength of the concrete-rock bonds generated.

Last, during the dynamic shear evolution, there is a local competition of the shear resistance between the two interfaces, which can generate some unusual features in the shear evolution graph. For example, in Fig. 19 (b), there is a plateau (Fig. 19 (b), AB) in the shear evolution of one interface; this means that due to the local shear resistance of the interfaces and the competition of shear resistance between the two interfaces, at some point in the shear history, the shear loading focuses on one interface only.

4.2. Post-mortem analysis of concrete-rock interfaces

In complement to the description of the static and dynamic shear behavior of concrete-rock interfaces presented in Section 4.1, a post-mortem analysis was carried out to discuss the mechanisms driving the failure of concrete-rock interfaces.

Fig. 20 shows a typical shear failure of concrete-rock interfaces dynamically tested in this study.

From Fig. 20, it is clear that the shear failure occurs mainly along the interfaces (highlighted in red) and is accompanied by a significant shear displacement (highlighted in blue). This shear failure seems mainly driven by the failure of the concrete rock bonds. Similar observations can be presented for the shear failure of the sample presented in Fig. 20 (b). Overall, the shear failure obtained in this experimental study passes along the interfaces, mainly due to the lower normal stresses considered.

For further analysis, three test results performed as part of the exploratory work, carried out to assess the feasibility of the experimental methodology presented in this study, are discussed. The samples used in this exploratory work have a rock slab in the central part and concrete slabs cast at the extremities [50].

First, the mechanisms affecting the shear failure of concrete-rock interfaces under static conditions are discussed.

Fig. 21 shows three screenshots of a video recorded during a quasi-static test of rough concrete-granite interfaces with a maximum confinement stress of 2.5 MPa. The succession of the images in Fig. 21 (a), (b), and (c) shows that under lower normal loading, the shear behavior of concrete-rock interfaces is local and progressive, as

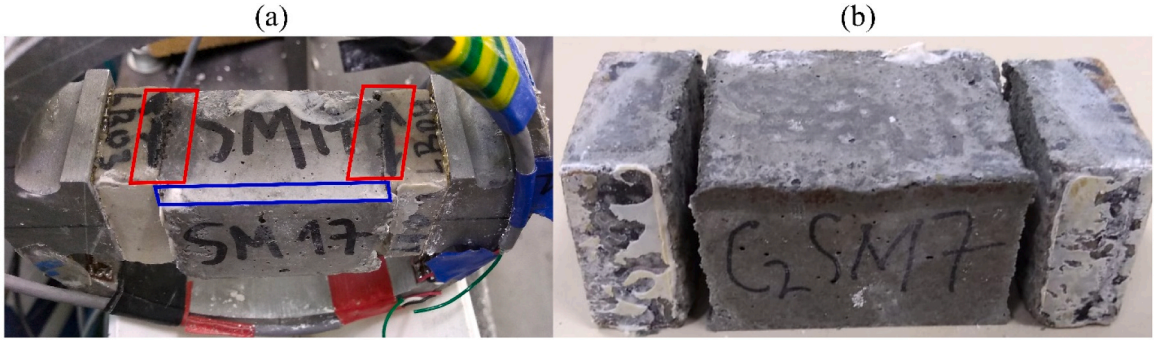

Fig. 20. Post-mortem analysis of concrete-rock interfaces submitted to dynamic shear loading carried out as part of the experimental study presented in this work.

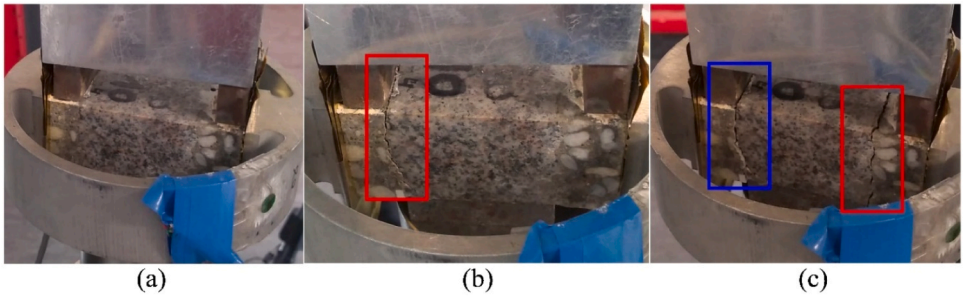

Fig. 21. Failure Initiation and propagation along the rough concrete-granite interfaces submitted to quasi-static loading and under confinement stress of 2.5 MPa; (a) no failure in either interface, (b) failure at the first interfaces, and (c) failure at the second interfaces.

described in Section 4.1. The failure seems to evolve first only on the interfaces with lower resistance (Fig. 21 (b)) and later in the more resistant interface (Fig. 21 (c)). The resistance of an interface is assumed to be dependent on the combined effect of roughness and strength of concrete-rock bonds. The failure occurs mainly along the interfaces without significant concrete or granite damage. This failure is driven principally by two principal mechanisms: the debonding of concrete-rock bonds and the influence of waviness (roughness). The waviness of the interfaces contributes to the shear resistance through surfaces interlocking and is responsible for the dilation of the sample. It is worth emphasizing that this discussion of the mechanisms active during the shear failure is sensitive to the normal stress level. This means that at higher normal stress (beyond the scope of this study), the shear failure might not necessarily evolve along the interface, which would consequently reduce the influence of concrete-rock bonds and lead to significant damage around the interface, principally through the weaker material or both materials.

Second, considering the mechanisms driving the failure of concrete-rock interfaces under dynamic conditions, a sample tested with a dynamic shear loading was retrieved from the confinement ring and later scanned using X-ray tomography. It is worth noting that the scanned sample was tested with the dynamic shear testing methodology presented in this study and in similar conditions but with a higher confinement stress (maximum confinement stress of around 8 MPa). The X-ray machine was used to scan three different sections perpendicular to the shear plane and located close to the two extremities and at the central part of the sample (Fig. 22).

The X-ray scans of these three sections are presented in Fig. 23. The analysis of these scans shows that, like the static shear failure of interfaces, the dynamic shear failure of rough concrete-rock interfaces occurs either along the interfaces or through the weaker material (concrete in this case) depending on parameters such as the normal stress, the roughness, and the concrete-rock bonds.

In Fig. 23 (a), the failure of the left interface of the sample occurs along the interface. This could indicate a shear failure driven mainly by the mechanisms associated with the concrete-rock bonds.

In Fig. 23 (b), the failure of the right interface seems to start to evolve along the interface (S1), encounters a single waviness characterizing the entire interface (S2 and S3), and then faces the competition of resistance between the strengthened interface (concrete-rock bonds and waviness), the rock and the concrete. The outcome of this competition leads to the propagation of failure through the concrete part of the sample because of its low resistance.

This post-mortem analysis of a concrete-rock sample tested using a dynamic shear loading is very similar to the one obtained for the sample tested using the static shear test. This indicates that the dynamic shear failure of concrete-rock interfaces is driven by the same mechanisms observed in the static shear failure.

The outcome of this post-mortem analysis has shown an interest in improving the experimental methodology proposed in this study to collect more information about the mechanisms driving the shear failure at the micro-fracture level around the interfaces. Such information could prove decisive in further understanding the complex mechanisms active during the shear failure of concrete-rock interfaces. Such improvement could include fast imaging techniques such as X-ray phase contrast imaging and X-ray digital image correlation. These two methods were used, for example, by Wang et al. [51], to investigate the fracture of concrete under dynamic loading. Furthermore, a high-speed camera could be included in the experimental methodology presented in this study to collect information that could prove useful in the damage and failure modes analysis as used in the experimental study performed by Li et al. [38].

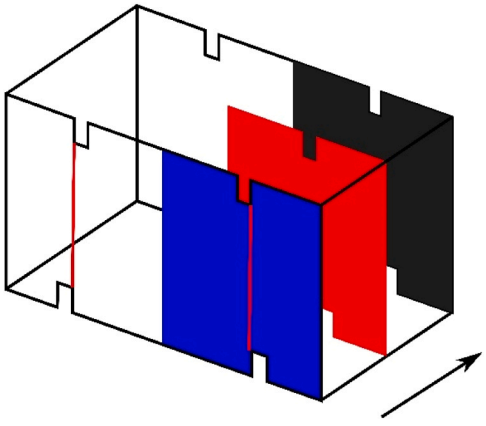

Fig. 22. Scanning schema: the three sections of interest are marked as blue, red, and black, and the two red vertical lines represent the two interfaces tested per sample.

4.3. Shear strength of concrete-rock interfaces in terms of normal stress

The evolution of the peak shear strength in terms of the normal stress for the three types of interfaces tested is presented in Fig. 24. The normal stress corresponds to the value recorded when the shear stress reaches a peak.

Each square in Fig. 24 represents the dynamic peak shear strength and normal stress of one interface, while each dot represents the static peak shear strength and normal stress of one interface.

The correlation coefficient between the static peak shear strength and the normal stress is 0.60 for the smooth concrete-sandstone, 0.99 for the bush-hammered concrete-granite, and 0.56 for the rough concrete-granite interfaces. The correlation coefficient of the bush-hammered concrete-granite interfaces is higher than that of the smooth concrete-sandstone interfaces. This comparison could indicate that the bush-hammered granite surfaces have a similar distribution of micro-roughness locally. This distribution of micro-roughness leads to similar local strength of concrete-rock bonds.

Only a qualitative assessment is possible for the correlation between

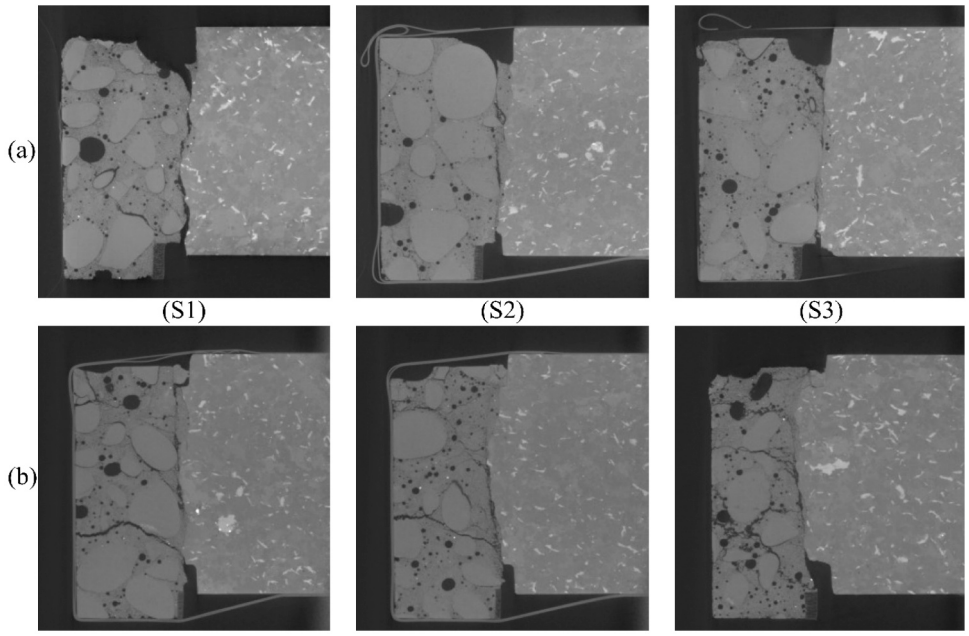

Fig. 23. X -rays scans of concrete-rock interfaces: S1 and S3 are the scans of the sections at the extremities, and S2 is at the central part of the sample, (a) left interface, and (b) right interface
(Modified from DeLucia et al. [50]).

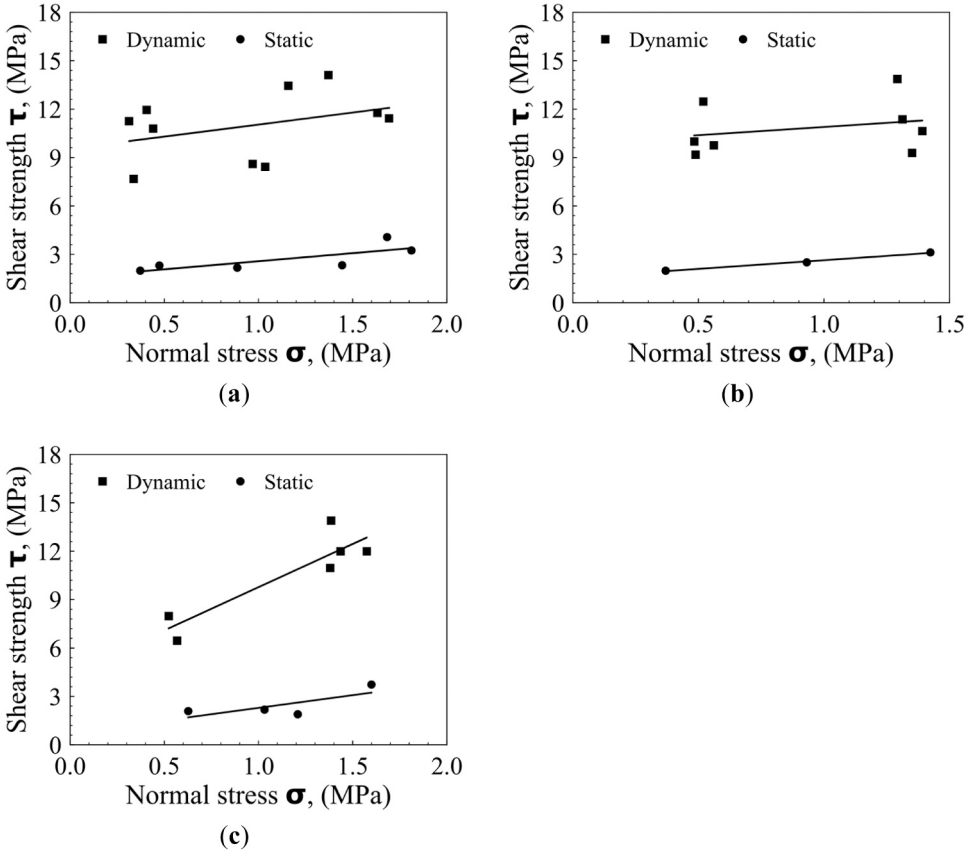

Fig. 24. Peak shear strength per normal stress: (a) smooth concrete-sandstone, (b) bush-hammered concrete-granite, and (c) rough concrete-granite interfaces.

the static peak shear strength and the normal stress of the rough concrete-granite interfaces because the peak shear strength of these interfaces depends on the roughness of the interfaces on top of the normal stress. Furthermore, the roughness of the interfaces tested is not equal.

The correlation coefficient between the dynamic peak shear strength and the normal stress is 0.14 for the smooth concrete-sandstone, 0.07 for the bush-hammered concrete-granite, and 0.81 for the rough concrete-granite interfaces. The correlation coefficients of smooth concrete-

sandstone interfaces and the bush-hammered concrete-granite interfaces are negligible. This comparison could indicate that within the range of normal stress considered in this experimental study (below 2 MPa), the dynamic peak shear strength of concrete-rock interfaces is poorly correlated with the normal stress.

The correlation coefficient of the rough concrete-granite is high (0.81). However, it is worth mentioning that the dynamic shear strength of each interface is influenced by the normal stress and the roughness. Since each interface tested has a different roughness, separating the influence of the normal stress from the roughness is not straightforward. Consequently, no definitive conclusion can be taken from this correlation coefficient. Nevertheless, it appears that the normal stress has a higher influence on the dynamic peak shear strength of the rough concrete-granite interfaces than on the dynamic peak shear strength of the other two interfaces. This observation is clear when one observes the inclination of the fitting lines in Fig. 24.

4.4. Influence of the roughness on the shear resistance of concrete-rock interfaces

Characterizing the influence of roughness on the shear strength of interfaces (rock-rock and concrete-rock) is very complex. This complexity is evidenced by the fact that most of the breakthroughs achieved in understanding the shear behavior of interfaces are related to the proposition of roughness parameters and failure criteria [4,6,8]. In this study, three levels of interface roughness are tested. The results of the static and dynamic shear tests of bush-hammered concrete-granite interfaces (Fig. 10 (a) and Fig. 15 (a)) validate the conclusions obtained in previous studies stating that the formation of concrete-granite bonds depends on the existence of micro-roughness [21,52]. However, the results of static and dynamic shear tests of smooth concrete-sandstone interfaces (Fig. 9 (a) and Fig. 13 (a) and (b)) obtained in this study show that the surface chemistry of sandstone is enough for the formation of concrete-rock bonds and therefore there is no need for an addition of micro-roughness. This observation indicates that the roughness and the surface chemistry of the rock play complex roles in the formation of concrete-rock bonds.

Furthermore, the results of the static and dynamic shear tests of rough concrete-granite interfaces (Fig. 24 (c)) show that the combined effect of roughness and normal stress seems to play a significant role in the shear resistance of interfaces.

4.5. Comparative assessment of the static and dynamic shear resistance of concrete-rock interfaces

For all the interfaces tested, the dynamic peak shear strength is at least three to four times higher than the static peak shear strength (Fig. 24). This difference indicates that the shear resistance of concrete-rock interfaces with low confinement stress is strain rate sensitive. However, the sensitivity of the mechanical resistances of geomaterial with the loading rate is not new. Concrete and rock as intact materials have been found to have higher compressive and tensile strength when tested with a dynamic loading than with a static loading. This mechanical resistance increase is called the dynamic increase factor (DIF). The structural effect is sometimes presented as the cause of the DIF for geomaterial submitted to uniaxial compression loading. For geomaterials tested in tension, the DIF is suggested to be related to the material and, principally, the micro-fracture level [53]. This study suggests that the combination of the structural effect and the micro-cracking close to the concrete-rock interface likely explains the DIF obtained. The micro-cracking is likely due to the restrained shrinkage of concrete. Furthermore, this micro-cracking might also be affected by the roughness of the rock surface. This proposition is based on the fact that the shear behavior investigated in this study is carried out under a defined confinement loading and includes an important influence on roughness.

In Fig. 25, the results of the static and dynamic shear resistance of the bush-hammered concrete-granite and smooth concrete-sandstone interfaces tested in this study are plotted against the normal stress when the shear stress reaches a peak. In the same graph, the results of the static and dynamic tensile strength of the concrete-limestone interfaces without confinement stress presented by Zhou et al. [39] are plotted against the inclination of the interface during the test.

Each filled square and filled dot in Fig. 25 represents a static and dynamic shear resistance of an interface in terms of the normal stress (lower x-axis). Each unfilled square and unfilled dot represent, respectively, the static and the dynamic tensile strength of an interface in terms of the inclination of the interface (upper x-axis).

Fig. 25 shows that the dynamic tensile strength of the concrete-limestone interface is at least five times higher than the static tensile strength of the same interface. This indicates that different DIFs are obtained for different types of loading.

Furthermore, from the results obtained in this study and other literature, it appears that the DIF of geomaterials submitted to shear loading depends on whether the sample is an intact material or a combination of two materials. A DIF varying around two can be found in the literature [34] for intact concrete, while a value between three and four is obtained in this study for concrete-rock samples. It is worth emphasizing that the failure of the concrete-rock samples tested in this study occurred mainly across the interfaces. This means that the location of the failure could be the other factor influencing the DIF of geomaterials submitted to shear loading.

5. Conclusion

In this experimental study, the investigation of the static and dynamic shear behavior of concrete-rock interfaces under low confinement stresses was carried out. The test setup used in static and dynamic tests maintains the basic concepts of the conventional direct shear test. In both tests, the confinement stress is applied using a confinement ring. For the static test, the shear loading is applied using an electromechanical press. For the dynamic test, the shear loading is applied using the split Hopkinson pressure bar system consisting of two output bars and one input bar. Three types of interfaces formed by two types of rocks are tested: the smooth sandstone interfaces, the bush-hammered granite interfaces, and the rough granite interfaces.

The results of the static shear tests showed that the shear evolution can be separated into three stages: the shear stress accumulation, the shear slip, and the residual shear stress stage. The concrete-rock bonds drive the shear evolution in the shear stress accumulation stage; the transition from concrete-rock bonds to friction directs the shear slip stage, while residual friction is the main mechanism in the residual shear stress stage. The similarity of this description to the description of shear tests carried out using the conventional direct shear test set the static shear test presented as a possible alternative to the conventional direct shear test. Furthermore, the results of the static shear tests show that the surface chemistry and the roughness of the rock surface influence the formation of concrete-rock bonds.

The results of the dynamic shear tests reveal that the dynamic shear evolution can also be separated into the three stages observed in the static tests. However, different from the static shear test, it appears that the roughness of the interface and friction drive the first and second stages.

Furthermore, the dynamic shear resistance of concrete-rock interfaces submitted to low normal stresses not exceeding 2 MPa does not depend substantially on the normal stresses. Meanwhile, it is worth reporting that roughness and normal stress influence the dynamic shear resistance of concrete-rock interfaces.

From the preliminary comparative assessment of the static and dynamic shear resistance of concrete-rock interfaces under low confinement stress, the dynamic peak shear strength of the concrete-rock interfaces is three to four times higher than their static counterparts.

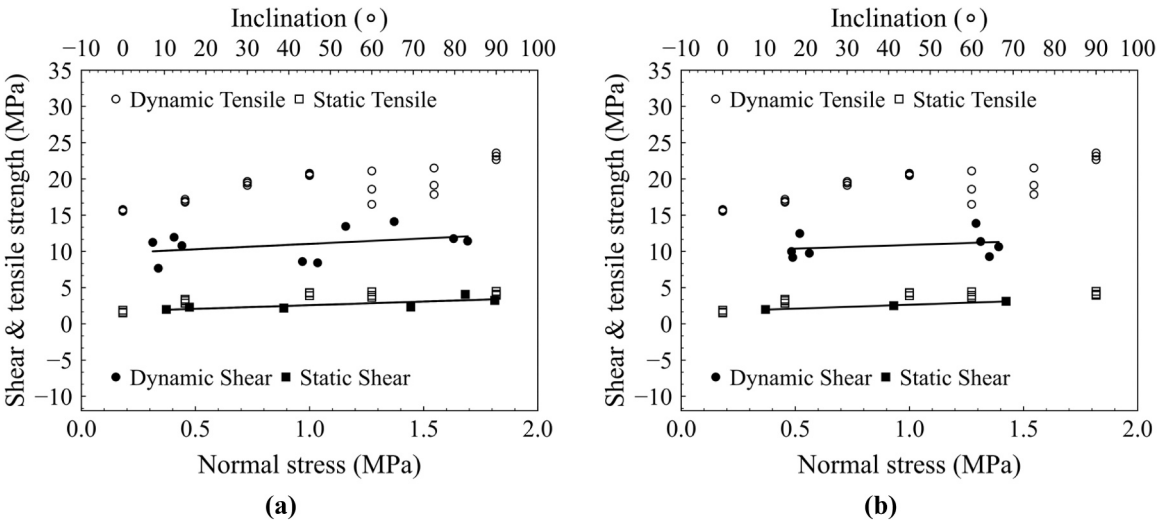

Fig. 25. Static - dynamic shear resistance of interfaces and static - dynamic tensile resistances of interfaces: (a) smooth concrete-sandstone and (b) bush-hammered concrete-granite.

This increase in the shear strength is attributed to the structural effect combined with the bonds and roughness on the shear resistance.

This study is one of the first in the literature to investigate the dynamic shear behavior of interfaces. Despite its achievement, more work is required to understand better the dynamic shear behavior of interfaces. The experimental methodology presented in this study should be improved to enhance the characterization of the mechanisms driving the dynamic shear behavior of interfaces. Such an improvement could include an imaging technique to collect the displacement fields across the interfaces. This information could lead to a better interpretation of the role of roughness, normal stress, and the strength of concrete-rock bonds in the dynamic shear behavior of concrete-rock interfaces. Besides the experimental methodology, other special investigations focused separately on the influence of roughness, rock lithologies, different ranges of normal stresses, and the scale effect are required before providing guidelines for application in engineering projects.

Funding

The Doctoral School IMEP2, Université Grenoble Alpes, France, funded this research project.

CRediT authorship contribution statement

Pascal Forquin: Methodology, Resources, Writing – review & editing. **Sophie Capdevielle:** Conceptualization, Investigation, Methodology, Resources, Supervision, Visualization, Writing – review & editing. **Menes Badika:** Writing – review & editing, Writing – original draft, Visualization, Validation, Methodology, Investigation, Formal analysis, Data curation, Conceptualization. **Matthieu Briffaut:** Writing – review & editing, Supervision, Resources, Methodology, Conceptualization. **Dominique Saletti:** Writing – review & editing, Supervision, Conceptualization, Investigation, Methodology, Resources.

Declaration of Competing Interest

The authors declare that they have no known competing financial interests or personal relationships that could have appeared to influence the work reported in this paper.

Data availability

Data will be made available on request.

References

[1] Sujatha V, Kishen JMC. Energy release rate due to friction at bimaterial interface in dams. J Eng Mech 2003;vol. 129(7):793–800. https://doi.org/10.1061/(ASCE)0733-9399(2003)129:7(793).
[2] Fishman YA. Features of shear failure of brittle materials and concrete structures on rock foundations. Int J Rock Mech Min Sci 2008;vol. 45(6):976–92. https://doi.org/10.1016/j.ijrmms.2007.09.011.
[3] Fishman YA. Stability of concrete retaining structures and their interface with rock foundations. Int J Rock Mech Min Sci 2009;vol. 46(6):957–66. https://doi.org/10.1016/j.ijrmms.2009.05.006.
[4] Patton FD. Multiple modes of shear failure in rock. 1st ISRM Congr 1966 1966:509–13.
[5] B. Ladany and G. Archambault, Simulation of Shear Behavior of a Jointed Rock Mass, no. January 1969, pp. 105–125, 1969.
[6] Barton N, Choubey V. The shear strength of rock joints in theory and practice. Rock Mech Felsmech Mec Des Roches 1977;vol. 10(1–2):1–54. https://doi.org/10.1007/BF01261801.
[7] Tse R, Cruden DM. Estimating joint roughness coefficients. Int J Rock Mech Min Sci Geomech Abstr 1979;vol. 16(5):303–7. https://doi.org/10.1016/0148-9062(79)90241-9.
[8] Grasselli G, Egger P. Constitutive law for the shear strength of rock joints based on three-dimensional surface parameters. Int J Rock Mech Min Sci 2003;vol. 40(1):25–40. https://doi.org/10.1016/S1365-1609(02)00101-6.
[9] Grasselli G. Manuel rocha medal recipient shear strength of rock joints based on quantified surface description. Rock Mech Rock Eng 2006;vol. 39(4):295–314. https://doi.org/10.1007/s00603-006-0100-0.
[10] Tang ZC, Zhang ZF, Zuo CQ, Jiao Y-Y. Peak shear strength criterion for mismatched rock joints: revisiting JRC-JMC criterion. Int J Rock Mech Min Sci 2021;vol. 147:104894. https://doi.org/10.1016/j.ijrmms.2021.104894.
[11] El-Soudani SM. Profilometric analysis of fractures. Metallography 1978;vol. 11(3):247–336. https://doi.org/10.1016/0026-0800(78)90045-9.
[12] Lanaro F. A random field model for surface roughness and aperture of rock fractures. Int J Rock Mech Min Sci Dec. 2000;vol. 37(8):1195–210. https://doi.org/10.1016/S1365-1609(00)00052-6.
[13] Indraratna B, Haque A. Experimental study of shear behavior of rock joints under constant normal stiffness conditions. Int J Rock Mech Min Sci 1997;vol. 34(3–4):141.e1–141.e14. https://doi.org/10.1016/S1365-1609(97)00068-3.
[14] Krounis A, Johansson F, Larsson S. Shear strength of partially bonded concrete–rock interfaces for application in dam stability analyses. Rock Mech Rock Eng 2016;vol. 49(7):2711–22. https://doi.org/10.1007/s00603-016-0962-8.
[15] Saiang D, Malmgren L, Nordlund E. Laboratory tests on shotcrete-rock joints in direct shear, tension and compression. Rock Mech Rock Eng 2005;vol. 38(4):275–97. https://doi.org/10.1007/s00603-005-0055-6.
[16] Moradian ZA, Ballivy G, Rivard P. Application of acoustic emission for monitoring shear behavior of bonded concrete–rock joints under direct shear test. Can J Civ Eng 2012;vol. 39(8):887–96. https://doi.org/10.1139/l2012-073.
[17] Tian HM, Chen WZ, Yang DS, Yang JP. Experimental and numerical analysis of the shear behaviour of cemented concrete–rock joints. Rock Mech Rock Eng 2015;vol. 48(1):213–22. https://doi.org/10.1007/s00603-014-0560-6.
[18] Mouzannar H, Bost M, Leroux M, Virely D. Experimental study of the shear strength of bonded concrete–rock interfaces: surface morphology and scale effect. Rock Mech Rock Eng 2017;vol. 50(10):2601–25. https://doi.org/10.1007/s00603-017-1259-2.

[19] Bost M, Mouzannar H, Rojat F, Coubard G, Rajot J-P. Metric scale study of the bonded concrete-rock interface shear behaviour. KSCE J Civ Eng 2020;vol. 24(2): 390–403. https://doi.org/10.1007/s12205-019-0824-5.
[20] Bista D, Sas G, Johansson F, Lia L. Influence of location of large-scale asperity on shear strength of concrete-rock interface under eccentric load. J Rock Mech Geotech Eng 2020;vol. 12(3):449–60. https://doi.org/10.1016/j.jrmge.2020.01.001.
[21] Badika M, El Merabi B, Capdevielle S, Dufour F, Saletti D, Briffaut M. Influence of concrete–rock bonds and roughness on the shear behavior of concrete–rock interfaces under low normal loading, experimental and numerical analysis. Appl Sci 2022;vol. 12(11):5643. https://doi.org/10.3390/app12115643.
[22] Moradian ZA, Ballivy G, Rivard P, Gravel C, Rousseau B. Evaluating damage during shear tests of rock joints using acoustic emissions. Int J Rock Mech Min Sci 2010; vol. 47(4):590–8. https://doi.org/10.1016/j.ijrmms.2010.01.004.
[23] Zhang QB, Zhao J. A review of dynamic experimental techniques and mechanical behaviour of rock materials. Rock Mech Rock Eng 2014;vol. 47(4):1411–78. https://doi.org/10.1007/s00603-013-0463-y.
[24] Hutson RW, Dowding CH. Joint asperity degradation during cyclic shear. Int J Rock Mech Min Sci Geomech Abstr 1990;vol. 27(2):109–19. https://doi.org/10.1016/0148-9062(90)94859-R.
[25] Lee H, Park Y, Cho T, You K. Influence of asperity degradation on the mechanical behavior of rough rock joints under cyclic shear loading. Int J Rock Mech Min Sci 2001;vol. 38(7):967–80. https://doi.org/10.1016/S1365-1609(01)00060-0.
[26] Mirzaghorbanali A, Nemcik J, Aziz N. Effects of shear rate on cyclic loading shear behaviour of rock joints under constant normal stiffness conditions. Rock Mech Rock Eng 2014;vol. 47(5):1931–8. https://doi.org/10.1007/s00603-013-0453-0.
[27] Dai F, Huang S, Xia K, Tan Z. Some fundamental issues in dynamic compression and tension tests of rocks using split hopkinson pressure bar. Rock Mech Rock Eng 2010;vol. 43(6):657–66. https://doi.org/10.1007/s00603-010-0091-8.
[28] Wang H-C, Zhao J, Li J, Liu K, Braithwaite CH, Zhang Q-B. Dynamic mechanical properties and fracturing behaviour of concrete under biaxial compression. Constr Build Mater 2021;vol. 301:124085. https://doi.org/10.1016/j.conbuildmat.2021.124085.
[29] Dai F, Xia K, Luo SN. Semicircular bend testing with split Hopkinson pressure bar for measuring dynamic tensile strength of brittle solids. Rev Sci Instrum 2008;vol. 79(12):123903. https://doi.org/10.1063/1.3043420.
[30] Huang S, Chen R, Xia KW. Quantification of dynamic tensile parameters of rocks using a modified Kolsky tension bar apparatus. J Rock Mech Geotech Eng 2010;vol. 2(2):162–8. https://doi.org/10.3724/SP.J.1235.2010.00162.
[31] Huang S, Feng XT, Xia K. A dynamic punch method to quantify the dynamic shear strength of brittle solids. Rev Sci Instrum 2011;vol. 82(5):053901. https://doi.org/10.1063/1.3585983.
[32] P. Forquin and L. Sallier, A Testing Technique to Characterise the Shear Behaviour of Concrete at High Strain-Rates, 2013, pp. 531–536. doi:10.1007/978–1-4614–4238-7_68.
[33] Lukić B, Forquin P. Experimental characterization of the punch through shear strength of an ultra-high performance concrete. Int J Impact Eng 2016;vol. 91: 34–45. https://doi.org/10.1016/j.ijimpeng.2015.12.009.
[34] Abdul-Rahman R, Saletti D, Forquin P. Experimental study of the static and dynamic behavior of pre-stressed concrete subjected to shear loading. Eng Struct 2021;vol. 234:111865. https://doi.org/10.1016/j.engstruct.2021.111865.
[35] Tawfik A, Curosu I, Alsous G, Mechtcherine V. A testing device to investigate the properties of strain-hardening, cement-based composites (SHCC) under impact shear loading. Int J Impact Eng 2022;vol. 167:104280. https://doi.org/10.1016/j.ijimpeng.2022.104280.
[36] Dai F, Xia K, Zheng H, Wang YX. Determination of dynamic rock Mode-I fracture parameters using cracked chevron notched semi-circular bend specimen. Eng Fract Mech 2011;vol. 78(15):2633–44. https://doi.org/10.1016/j.engfracmech.2011.06.022.
[37] Zhang QB, Zhao J. Determination of mechanical properties and full-field strain measurements of rock material under dynamic loads. Int J Rock Mech Min Sci 2013;vol. 60:423–39. https://doi.org/10.1016/j.ijrmms.2013.01.005.
[38] Li J, Yuan W, Li H, Zou C. Study on dynamic shear deformation behaviors and test methodology of sawtooth-shaped rock joints under impact load. Int J Rock Mech Min Sci 2022;vol. 158:105210. https://doi.org/10.1016/j.ijrmms.2022.105210.
[39] Zhou Z, Lu J, Cai X. Static and dynamic tensile behavior of rock-concrete bi-material disc with different interface inclinations. Constr Build Mater 2020;vol. 256:119424. https://doi.org/10.1016/j.conbuildmat.2020.119424.
[40] Qiu H, Chen B, Wang F, Liao F, Wang M, Wan D. Investigating dynamic fracture in marble-mortar interface under impact loading. Constr Build Mater 2022;vol. 336: 127548. https://doi.org/10.1016/j.conbuildmat.2022.127548.
[41] Forquin P, Abdul-Rahman R, Saletti D. A novel experimental method to characterise the shear strength of concrete based on pre-stressed samples. Strain 2022;vol. 58(2). https://doi.org/10.1111/str.12407.
[42] G. Grasselli, Shear strength of rock joints based on quantified surface description, Ecole polytechnique federale de lausanne, 2001. [Online]. Available: ⟨https://infoscience.epfl.ch/record/32880?ln=en⟩.
[43] Tatone BSA, Grasselli G. A method to evaluate the three-dimensional roughness of fracture surfaces in brittle geomaterials. Rev Sci Instrum 2009;vol. 80(12):125110. https://doi.org/10.1063/1.3266964.
[44] Gabet T, Malécot Y, Daudeville L. Triaxial behaviour of concrete under high stresses: influence of the loading path on compaction and limit states. Cem Concr Res 2008;vol. 38(3):403–12. https://doi.org/10.1016/j.cemconres.2007.09.029.
[45] Piotrowska E, Forquin P, Malecot Y. Experimental study of static and dynamic behavior of concrete under high confinement: Effect of coarse aggregate strength. Mech Mater 2016;vol. 92:164–74. https://doi.org/10.1016/j.mechmat.2015.09.005.
[46] Vu XH, Malecot Y, Daudeville L, Buzaud E. Experimental analysis of concrete behavior under high confinement: Effect of the saturation ratio. Int J Solids Struct 2009;vol. 46(5):1105–20. https://doi.org/10.1016/j.ijsolstr.2008.10.015.
[47] Erzar B, Forquin P. Analysis and modelling of the cohesion strength of concrete at high strain-rates. Int J Solids Struct 2014;vol. 51(14):2559–74. https://doi.org/10.1016/j.ijsolstr.2014.01.023.
[48] Muralha J, Grasselli G, Tatone B, Blümel M, Chryssanthakis P, Yujing J. ISRM suggested method for laboratory determination of the shear strength of rock joints: revised version. Rock Mech Rock Eng 2014;vol. 47(1):291–302. https://doi.org/10.1007/s00603-013-0519-z.
[49] Gary G, Mohr D. Modified kolsky formulas for an increased measurement duration of SHPB systems. Exp Mech 2013;vol. 53(4):713–7. https://doi.org/10.1007/s11340-012-9664-7.
[50] D. De Lucia, D. Saletti, M. Briffaut, and P. Forquin, quasi-static and dynamic loadings Cohesive shear strength of concrete-rock joints: a preliminary study in quasi-static and dynamic loadings, 2020, pp. 2–6.
[51] Wang HC, et al. In-situ deformation and fracturing characteristics of geomaterials under dynamic loading: insights from ultra-high-speed X-ray phase contrast imaging and DEM modelling. Int J Rock Mech Min Sci 2024;vol. 175:105656. https://doi.org/10.1016/j.ijrmms.2024.105656.
[52] Dong W, Wu Z, Zhang B, She J. Study on shear–softening constitutive law of rock–concrete interface. Rock Mech Rock Eng 2021;vol. 54(9):4677–94. https://doi.org/10.1007/s00603-021-02536-6.
[53] Li X, Chen Q, Chen J-F, Liao J, Lu Y. Dynamic increase factor (DIF) for concrete in compression and tension in FE modelling with a local concrete model. Int J Impact Eng 2022;vol. 163:104079. https://doi.org/10.1016/j.ijimpeng.2021.104079.